ELSEVIER

Journal of Chromatography A, 867 (2000) 1–21

JOURNAL OF CHROMATOGRAPHY A

www.elsevier.com/locate/chroma

Modeling of separations by closed-loop steady-state recycling chromatography of a racemic pharmaceutical intermediate

Igor Quiñones[a,b,c], Charles M. Grill[d], Larry Miller[e], Georges Guiochon[a,c,*]

[a]*Department of Chemistry, University of Tennessee, Knoxville, TN 37996-1600, USA*
[b]*Department of Chemical Engineering, University of Tennessee, Knoxville, TN 37996-1600, USA*
[c]*Division of Chemical and Analytical Sciences, Oak Ridge National Laboratory, Oak Ridge, TN 37831-6120, USA*
[d]*R&S Technology, 350 Columbia St., Wakefield, RI 02882-0352, USA*
[e]*Searle, 4901 Searle Parkway, Skokie, IL 60077, USA*

Received 16 August 1999; received in revised form 21 October 1999; accepted 25 October 1999

Abstract

Closed-loop steady-state recycling (SSR) is a cyclic, one-column process that is similar to simulated moving bed (SMB) chromatography in several respects. Both processes are cyclic. In both SMB and SSR, fractions are collected from the leading and trailing portions of the circulating chromatographic profile, and fresh sample is injected into the interior of the profile. However, SMB is a continuous process whereas SSR is a discontinuous, repetitive process. This paper presents a model for the closed-loop SSR process and its experimental validation in a case of practical importance. For this last purpose, we used the closed-loop SSR separation of the enantiomers of a racemic pharmaceutical intermediate. The experimental determination of the competitive adsorption equilibria was performed by frontal analysis in a system composed of a chiral HPLC column as the stationary phase and pure acetonitrile as the mobile phase. All the adsorption data were well correlated by the Langmuir model. The Langmuir model was used to calculate overloaded band profiles corresponding to the separation of racemic mixtures at both analytical and preparative scales. Theoretical band profiles were calculated using the equilibrium–dispersive model. With proper corrections for the contributions of the sources of extra-column band broadening, the model properly predicts the experimental band profiles obtained in the closed-loop SSR setup and demonstrates that a cyclic steady-state develops after the completion of a finite number of cycles. The results also show that the extra-column effects must be accounted for in order to model the closed-loop SSR process accurately.

Keywords: Steady-state recycling; Enantiomer separation; Pharmaceutical analysis; Mathematical modelling

1. Introduction

Enantiomeric separations are important for the pharmaceutical industry [1] and the topic of numerous recent papers [1–11]. These separations are difficult because they require a chiral selector and the enantioselectivity is often relatively low. This is why recycling has long been regarded as an attractive method of improving the quality of enantioseparations obtained by preparative chromatography [12,13]. Recycling can be implemented in different ways. The most popular modes are: (i) closed-loop;

*Corresponding author. Tel.: +1-423-974-0733; fax: +1-423-974-2667.
E-mail address: guiochon@utk.edu (G. Guiochon)

0021-9673/00/$ – see front matter
PII: S0021-9673(99)01128-0

(ii) alternate pumping; (iii) recycling of an intermediate cut; and (iv) recycling of the second peak tail [2,11]. Some of these techniques allow the introduction of fresh sample during each cycle, after the reinjection of the recycled fractions [3]. Various combinations of these techniques are of course possible. Recycling techniques usually improve recovery yield, decrease pressure drop and solvent consumption and increase production rate compared to conventional overloaded chromatography [3,14].

Recycling could be particularly useful for the separation of racemic mixtures [3–5,11]. Recently, a new technique, closed-loop steady-state recycling (SSR), was suggested [4,5]. Closed-loop SSR is similar to simulated moving bed (SMB) chromatography in that sample is injected into the interior of the circulating chromatographic profile and fractions are collected from the leading and the trailing portions of the profile. Unlike SMB, closed-loop SSR is not a continuous process; rather the SSR events occur sequentially and periodically. Thus, during a typical cycle, the fraction from the leading portion of the profile will be collected; later fresh sample will be injected at the appropriate point in the profile, and finally a certain fraction(s) from the trailing portion of the profile will be collected.

SMB reaches what was described as a periodic steady-state [15] or cyclic steady-state [16]. Closed-loop SSR reaches a similar periodic or cyclic steady-state [4,5]. It has become customary to refer to SMB as a ''steady-state'' process. However, it is recognized that this statement is merely short hand for cyclic or periodic steady-state. We will follow the same convention in this paper: whenever we refer to the attainment of steady-state in the SSR process, we are referring to the cyclic or periodic steady-state described above.

When SMB and SSR reach their respective cyclic steady-states, each process has major advantages relative to the conventional modes of HPLC. At cyclic steady-state, both SMB and SSR will generally have higher production rates, higher recoveries, and lower solvent usage than HPLC [5,17]. SMB, however, appears to have a lower solvent usage than SSR for a given separation [5].

Mathematical models were developed for the description of specific recycling techniques [3,11,14]. Accurate predictions of the associated band profiles were obtained using the equilibrium–dispersive model and the relevant equilibrium data [3]. In this study, we present a model for the closed-loop SSR process. The model could be useful for the method development, the scale-up and the optimization of separations performed using the SSR process.

2. Experimental

2.1. Equipment

2.1.1. Analytical scale

Chromatographic data, including analytical chromatograms, overloaded band profiles and breakthrough curves were acquired at the University of Tennessee using a HP 1100 series modular liquid chromatograph (Hewlett-Packard, Palo Alto, CA, USA). This instrument is composed of an isocratic pump, a Rheodyne 7725i injector (Cotati, CA, USA), a vacuum degasser for the mobile phase, a variable-wavelength detector, and a temperature-controlled column compartment. Personal computer-based software was used to control these modules and to acquire and process the UV signal.

2.1.2. Preparative scale

The closed-loop SSR experiments were performed at R&S Technology using a NovaPrep/SteadyCycle 200 system (R&S Technology, Wakefield, RI, USA). This instrument is composed of a NovaPrep 200 mobile phase pump with a maximum flow-rate of 200 ml min^{-1} and a maximum operating pressure of 2500 p.s.i. (1 p.s.i. = 6894.76 Pa); a variable-wavelength UV detector equipped with a high-pressure flow cell (Hitachi Instruments, San Jose, CA, USA); a six-port, air-actuated injection valve (Rheodyne, Cotati, CA, USA) with a 5.0 ml injection loop; several air actuated collection valves (Mace, Upland, CA, USA) and an injection metering pump Model B-100-S-4-2 (Eldex Labs, San Carlos, CA, USA). TurboPrep software (Merck, Darmstadt, Germany) was used to control the instrumentation.

All fractions were analyzed by analytical HPLC using an Hitachi L-6000 pump, a Rheodyne 6-way valve (model 7000L) equipped with a 20 μl loop and a Knauer variable-wavelength UV detector (Knauer,

Berlin, Germany). The peaks were integrated using a HP 3393A integrator (Hewlett-Packard).

2.2. Materials

A 250 mm×4.6 mm I.D. Chiralpak AS column (Chiral Technologies, Exton, PA, USA) was used to measure the adsorption data and the overloaded band profiles at the analytical scale. The adsorbent is amylose tris[(S)-α-methylbenzyl carbamate] coated on silica-gel. The particle size was 10 μm and the void fraction of the column was 0.77. A 250 mm× 20 mm I.D. Chiralpak AS column (Chiral Technologies) was used to perform the closed-loop SSR experiments. The particle size was 10 μm and the void fraction of the column (or total column porosity) was 0.73. It was derived from the retention time of the non-retained tracer, 1,3,5-tri-*tert*.-butyl benzene.

In all the experiments the mobile phase was acetonitrile (ACN). Acetonitrile was HPLC grade, purchased from Fisher Scientific (Pittsburgh, PA, USA). The solutes employed are proprietary compounds belonging to Searle (Searle, Skokie, IL, USA). We will use the indices 1 and 2 when referring to the first eluted enantiomer (E1) and second enantiomer (E2), respectively.

Table 1
Parameters of the separation under linear conditions

Parameter	First enantiomer	Second enantiomer
Analytical column (4.6×250 mm)		
k'	0.785	1.16
N	6600	5400
Preparative column (20×250 mm)		
k'	0.79	1.186
N	3721	3270

2.3. Procedures

2.3.1. Experimental study of the thermodynamics of the separation

The separation of the racemate under linear conditions is presented in Fig. 1. The parameters of the separation under linear conditions are reported in Table 1. In this table, k' is the retention factor and N the plate number.

The adsorption data were measured using the frontal analysis (FA) method, by pumping solutions of the single enantiomers or binary mixtures of the solutes in the mobile phase. After a breakthrough curve was recorded, the solution was replaced with one of higher concentration. The solutions were prepared and used on the same day. The column was

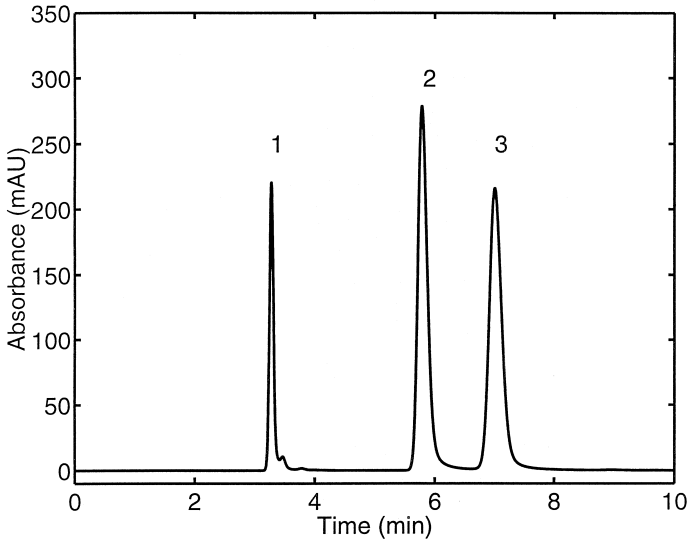

Fig. 1. Analytical separation of tri-*tert*.-butylbenzene (1), E1 (2) and E2 (3). Mobile phase is ACN. $T=22$°C, flow-rate is 1 ml min^{-1}, injected volume is 20 μl with a concentration of 0.5 g l^{-1}, UV detection at 225 nm.

held at 22°C. The signal was recorded at 254 nm. The flow-rate was 1 ml min^{-1}. For the mixtures of the two enantiomers, three different binary compositions were employed, with mass ratios of the two solutes equal to 1:3, 1:1 and 3:1. Ten different levels of total solute concentration were employed, the first level at 1 g l^{-1} and the last one at 10 g l^{-1}, with increments of 1 g l^{-1}.

2.3.2. Single solute isotherm data

The single-solute adsorption data measured by FA are presented in Figs. 2 and 3 (circles). In these figures the concentration in the mobile phase is represented by C and the concentration in the stationary phase is represented by q. Reported expressions [18] were used in order to calculate the adsorbed amounts from the FA data. The meaning of the lines is explained later (see section on modeling of adsorption isotherms). FA gives the concentration of component adsorbed on the surface of stationary phase at equilibrium as $q = C_{feed}(V_{bt} - V_0)/V_{sp}$, with C_{feed}, concentration of solution pumped into the column, V_{bt}, breakthrough volume, V_0, hold-up volume, and V_{sp}, volume of stationary phase in the column [18].

2.3.3. Binary solute isotherm data

In all the FA experiments, the initial concentration of the components was zero in the column. Thus, the concentration of the more retained enantiomer in the intermediate plateau was zero. Accordingly, there was no need to analyze the elute composition at this

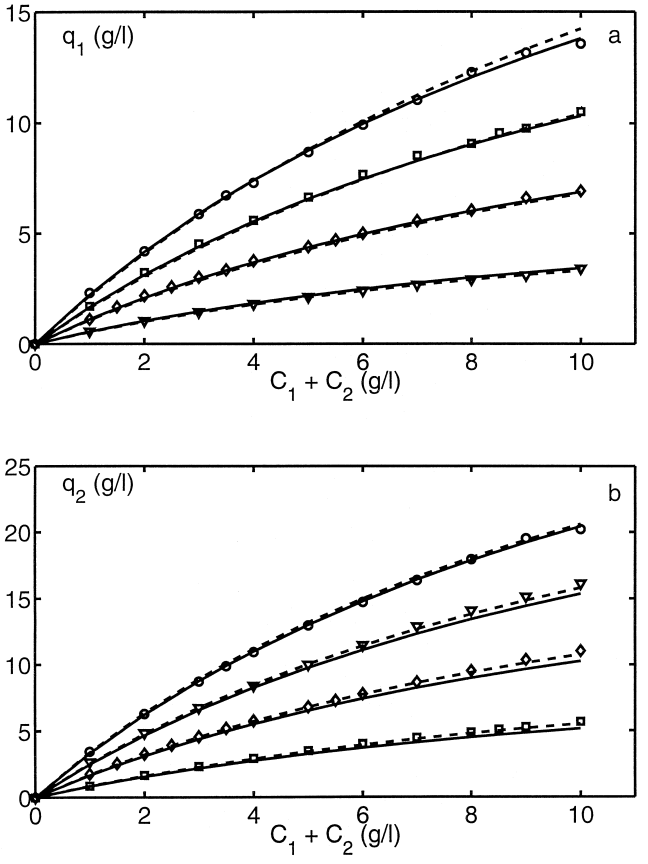

Fig. 2. Adsorbed amount of E1 (a) and E2 (b) determined using FA in their mixtures. Symbols: data for single solute, circles; data for 3:1 mixtures (three parts of E1 and one part of E2 in the mobile phase), squares; data for 1:1 mixtures, diamonds; and, data for 1:3 mixtures, triangles. The solid lines are the amounts calculated using Eq. (1) when using the parameters determined from single solute data. The dashed lines are the amounts calculated using Eq. (1) when using the parameters determined from the joint set of single and binary solute data.

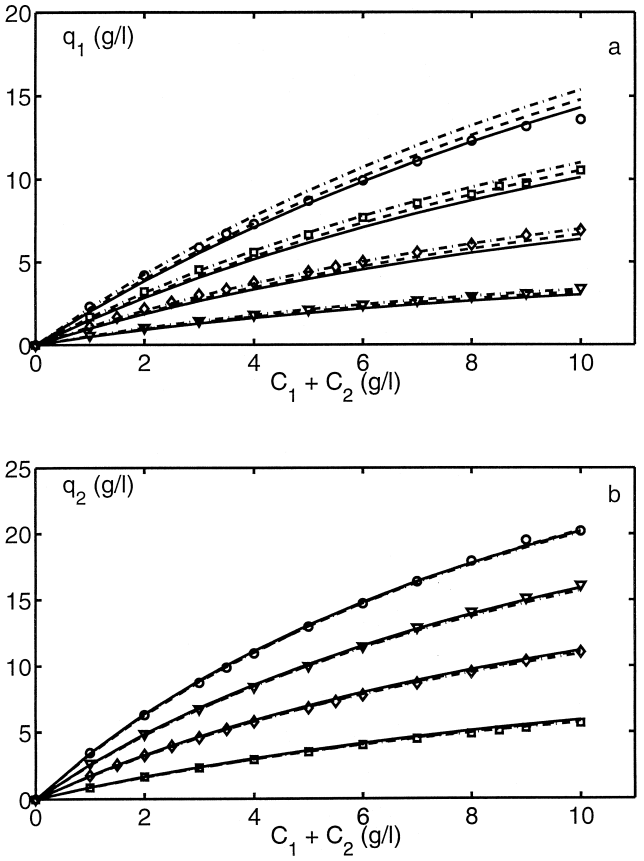

Fig. 3. Identical convention as in Fig. 2. The solid lines are the amounts calculated using Eq. (2) and the parameters determined from single solute data. The dashed lines are the amounts calculated using Eq. (2) and the parameters determined from the joint set of single and binary solute data. The dashed–dotted lines are the amounts calculated using Eq. (2) and the parameters determined from racemate data.

plateau [18]. The UV absorbance at the main FA plateaus was correlated with the feed concentrations using a second-order polynomial. This polynomial was employed to estimate the concentration of the least retained enantiomer in the intermediate subplateau. The retention times of both shocks (stepwise increase of the elute concentration), the hold-up time and the proper concentrations were inserted into the reported expressions [19] in order to derive the binary solute adsorption isotherm data. The adsorption data for the mixtures of the two enantiomers are also presented in Figs. 2 and 3 (squares, diamonds and triangles).

Due to the limited quantities of the pure enantiomers and the racemate available, only one adsorption data point per composition was measured for this system. The total absorption signal corresponding to two overloaded injections of the racemate were also measured. They are presented in Figs. 4 and 5 (dashed lines).

2.3.4. Preparative scale

Fig. 6 shows a schematic diagram of the closed-loop SSR setup. At the beginning of a run the injection loop (IL) is filled with sample by the injection pump (IP). The sample is drawn from the sample reservoir (SR). To accomplish this operation the injection valve (IV) is placed in the load position (dashed line flow path). Any excess of sample goes to waste through the port LW. At the same time, the mobile phase pump (MPP) draws mobile phase from the mobile phase reservoir (MPR) and pumps it

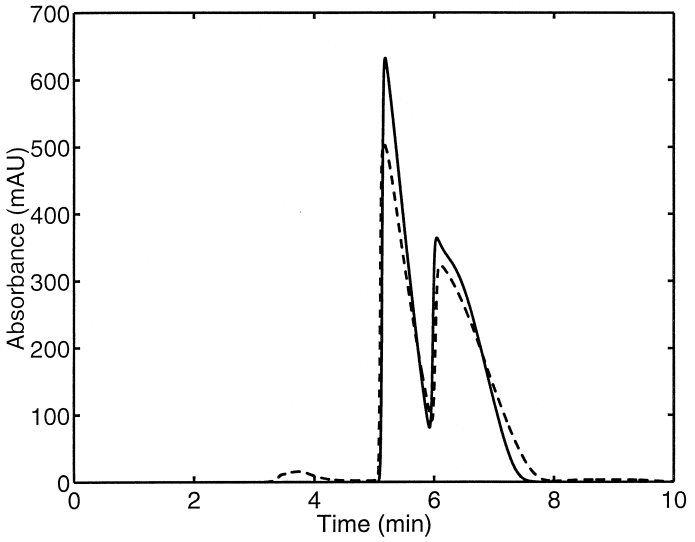

Fig. 4. Experimental (dashed line) and calculated (solid line) band profile of the racemate. Mobile phase is ACN. $T=22$°C, flow-rate is 1 ml min^{-1}, injected volume is 500 μl with a concentration of 5 g l^{-1}, UV detection at 254 nm.

through the column (C), through the UV detector (D), through the IV (dashed line flow path), through the collection valve manifold (CVM) and goes to waste through the waste valve (W).

The run starts by simultaneously placing the IV in the inject position (solid line flow path), opening the recycling valve (RV), and closing the waste valve (W). The sample in the IL is therefore transported by the mobile phase through the RV and the MPP onto the column. Once all the sample has been injected onto the column, the IV is switched back to the load position (dashed line flow path), the RV is closed and

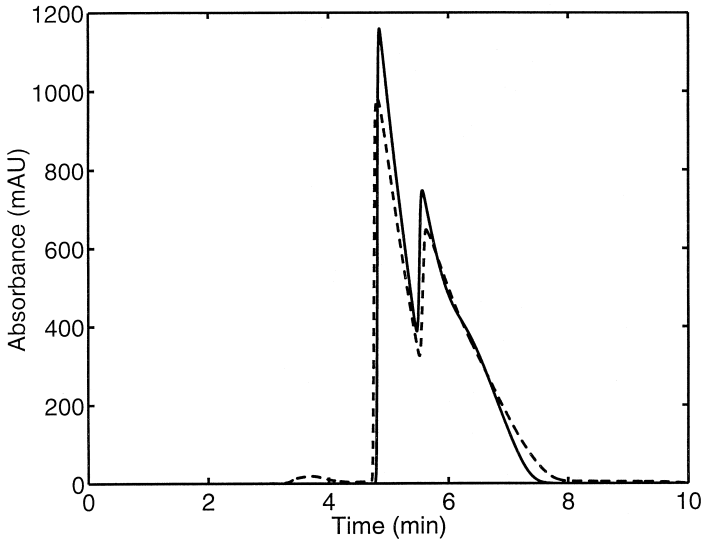

Fig. 5. Experimental (dashed line) and calculated (solid line) band profile of the racemate. Mobile phase is ACN. $T=22$°C, flow-rate is 1 ml min^{-1}, injected volume is 500 μl with a concentration of 10 g l^{-1}, UV detection at 254 nm.

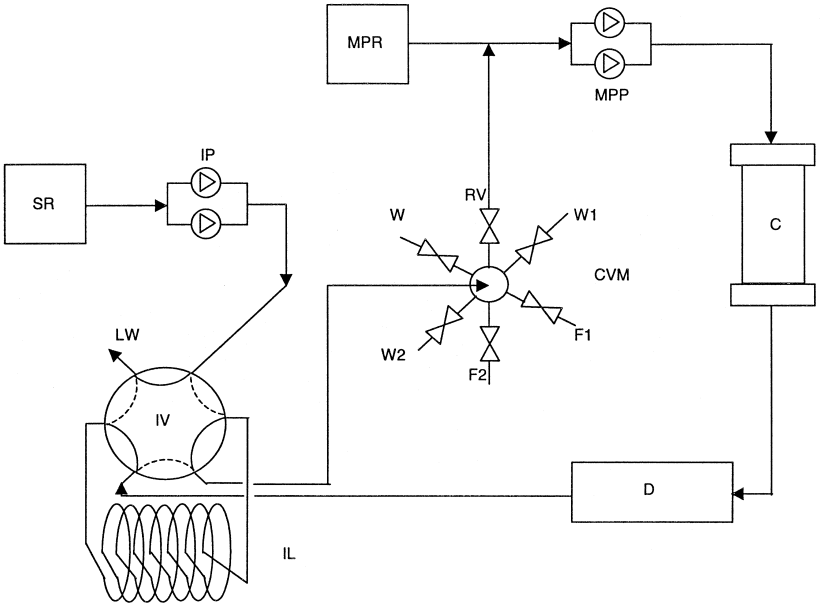

Fig. 6. Schematic diagram of the closed-loop SSR setup.

the W1 valve is opened, thus directing the effluent to waste. The IL is then filled again as described before.

When the leading edge of the profile is detected, valve F1 is opened and valve W1 is closed. Mobile phase continues to be drawn from the MPR. At the appropriate time, valve F1 is closed and the RV open. The collection of Fraction 1 is then complete. Simultaneously, the unresolved part of the circulating profile is directed to the column through the RV and the MPP.

At the appropriate time, as the central part of the profile elutes from the column, the IV is switched to the inject position (solid line flow path). This action diverts the effluent from the detector through the IL and fresh sample is injected into the interior of the profile.

At some specific time, valve F2 is open and the RV closed. This action starts the collection of Fraction 2 which lasts for some time until valve F2 is closed and valve W2 open. In a simultaneous fashion, the collection of Fraction 2 is concluded and the effluent is directed to waste (alternatively, this effluent can be collected as a very dilute fraction of E2). Then the cycle starts again with the detection of the profile leading edge. A more detailed explanation of the process can be found elsewhere [4].

In the experiments reported here, a relative time method was employed to control the operations of the instrument such as valve switching, pump operation, etc. With this procedure, the leading edge of the circulating profile is detected using the ascending height method. When the setpoint value is met, the collection valve for Fraction 1 (F1) is open, and the remaining time events are defined relative to the opening of F1. The flow-rate was 21.8 ml min^{-1}. The fresh sample of racemate had a concentration of 10 g l^{-1}.

The original absorption signal measured at 235 nm was converted into concentrations in order to compare the experimental results with the model results. It was assumed that the response of the detector is approximately linear in the studied concentration range. This assumption was verified at 254 nm. The experimental UV profile corresponding to the initial injection (circles) was divided by a factor which gives a concentration profile that upon integration produces the amount injected. The remaining profiles were then divided by the same factor. Note that the UV response of both enantiomers is the same.

For the last cycle (Cycle 20), fractions were collected every 10 s. The fractions were analyzed by HPLC using the instrument described earlier. The

mobile phase was acetonitrile and the flow-rate was 1 ml min^{-1}. The analytical column (250 mm×4.6 mm I.D.) was packed with 10 μm Chiralpak AS. The detector wavelength was set at 220 nm.

3. Theoretical

3.1. Adsorption equilibrium

The single solute and binary adsorption data were analyzed in terms of the Langmuir model [20]. The data were fitted to this model in two ways. In the first case, different adsorption capacities were assumed for each enantiomer (Fig. 2). In the second case, a common value of the saturation capacity was assumed (Fig. 3).

When different adsorption capacities are assumed for each enantiomer the isotherm model is defined as:

$$q_1 = \frac{n_1^{\infty} K_1^{L} C_1}{1 + K_1^{L} C_1 + K_2^{L} C_2} \quad (1a)$$

$$q_2 = \frac{n_2^{\infty} K_2^{L} C_2}{1 + K_1^{L} C_1 + K_2^{L} C_2} \quad (1b)$$

where q_i (g l^{-1}) is the concentration of the component adsorbed on the surface of the stationary phase, n_i^{∞} and K_i^{L} are the monolayer capacity and the equilibrium constant for the ith solute, respectively. Subscripts 1 and 2 correspond to the first and second enantiomer, respectively. When the single solute adsorption data are fitted to the Eq. (1) set, the parameters presented in the first row of Table 2 are obtained (''Single''). On the other hand, when the combined set of both single solute and binary adsorption data are fitted, the results shown in the second row of Table 2 are obtained (''All'').

When a common saturation capacity (n^{∞}) is assumed for both enantiomers, the isotherm model is defined as:

$$q_1 = \frac{n^{\infty} K_1^{L} C_1}{1 + K_1^{L} C_1 + K_2^{L} C_2} \quad (2a)$$

$$q_2 = \frac{n^{\infty} K_2^{L} C_2}{1 + K_1^{L} C_1 + K_2^{L} C_2} \quad (2b)$$

In this case the model is thermodynamically consistent [21]. Table 3 presents the parameters obtained when a unified value of the saturation capacity is assumed for both enantiomers. Three sets of parameters corresponding to three different situations were identified. In the first case the parameters were derived from the fit of the single solute data (first row, ''Single''). In the second case they were estimated from the fit of the combined set of single solute and competitive adsorption data (second row, ''All''). In the third case they were determined from the fit of the adsorption data obtained with the racemic mixture alone (third row, ''Racemate'').

3.2. Calculation of band profiles

For HPLC columns, which usually possess a high efficiency, the equilibrium–dispersive model is a good approximation to the solution of the system of mass balance equations that governs the separation process in the column [13]. In this case, the mass transfer in the column is assumed to be relatively fast, and the effects produced by the different resistances to mass transfer are lumped into an apparent Peclet number (Pe_{app}). Note that the equilibrium–dispersive model assumes that q_i and C_i are the equilibrium values related by the multicomponent adsorption isotherm.

For each component i in the column, the equilib-

Table 2
Fit of the experimental adsorption data to Eq. (1)

Data	n_1^{∞} (g/l)	$K_1^{L}\times10^2$ (l/g)	n_2^{∞} (g/l)	$K_2^{L}\times10^2$ (l/g)	F	RSS $(g/l)^2$
Single	32.8	7.28	47.9	7.45	1308.58	5.86
All	37.3	6.18	47.2	7.74	846.43	2.15

Table 3
Fit of the experimental adsorption data to Eq. (2)

Data	n^{∞} (g/l)	$K_1^{L}\times10^2$ (l/g)	$K_2^{L}\times10^2$ (l/g)	F	RSS $(g/l)^2$
Single	44.6	4.73	8.31	399.78	7.24
All	46.4	4.68	7.78	412.89	4.46
Racemate	44.5	5.29	8.26	1954.69	9.66

rium–dispersive model is represented by the following equation [22]:

$$\frac{\partial C_i}{\partial \theta} + \frac{\partial C_i}{\partial z} + \frac{(1-\epsilon)}{\epsilon} \cdot \frac{\partial q_i}{\partial \theta} = \frac{1}{\mathrm{Pe}_{\mathrm{app}}} \cdot \frac{\partial^2 C_i}{\partial z^2} \quad (3)$$

In this equation ϵ is the porosity of the packed bed and the non-dimensional position (z) is defined as ($z = x/L$) where x is the actual position in the direction of the flow and L is the column length. The non-dimensional time (θ) is defined by ($\theta = t/\tau$) where t is the actual time and τ is the residence or dead time defined by $\tau = L/u$, where u is the interstitial velocity in the packed bed. In Eq. (3) the apparent Peclet number is defined by $\mathrm{Pe}_{\mathrm{app}} = D_{\mathrm{ax}}/(uL) = 2N$, where N is the column plate number, an experimental parameter. The value of N is estimated from the chromatogram of an analytical injection (under linear conditions) of the solute of interest (Table 1).

The value of the partial derivatives $\partial q_i/\partial \theta$ are estimated from the adsorption isotherm for a system containing n solutes:

$$q_i = f(C_1, \ldots, C_i, \ldots, C_n) \quad (4)$$

Suitable boundary conditions are needed to solve Eq. (3). The column is assumed to be empty of solutes at the beginning of the process [$C_i(z,0) = 0$] and the boundary condition at the column inlet is defined by the profile leaving the chromatographic column at the end of the previous cycle and by the changes that this profile undergoes as a result of the peak shaving, the fresh sample injected, and extra-column dispersion and delay. The Eq. (3) set for the two enantiomers is solved numerically using a finite-differences algorithm. In this study, we apply a forward–backward finite differences procedure based on the Godunov scheme [23]. The equilibrium–dispersive model has been applied successfully to the description of single-solute and multisolute band profiles, provided that there exists an accurate description of the associated adsorption equilibrium [13].

3.3. Initial and boundary conditions

We showed previously [24] how important it is to account properly for the extra-column, non-ideal flow behavior in order to achieve a good prediction of the overloaded band profiles. The flow non-idealities are commonly represented by diffuse profiles like the ones originated in injection devices such as loops [25].

In the closed-loop SSR setup represented in Fig. 6, the extra-column, non-ideal flow behavior is a major factor affecting the overall outcome of the process. Two aspects of the problem are important. First, the bands leaving the column in cycle $i-1$ have to travel for some time before reentering the column in cycle i, so there is a time delay. Second, these bands receive additional dispersion when traveling through the tubings, valves, loop, pump and other devices. In order to estimate these effects, we removed the column from the setup presented in Fig. 6 and injected a tracer. From this experiment, we determined a total time delay of 0.77 min.

Afterwards, the overloaded band profiles were calculated using the equilibrium–dispersive model represented by Eq. (3). The parameters reported in Table 1 were used in the calculations, and the time delay was accounted for. The results of the experiments (circles) and the calculations (lines) for the initial pass and for the 5th cycle are presented in Figs. 7 and 8, respectively.

In order to include in the model not only the time delay but also the extra-column dispersion, we decided to represent the closed-loop SSR diagram depicted in Fig. 6 by the symbolic representation shown in Fig. 9. In this representation, we keep the chromatographic column with its parameters as it is in the real setup. On the other hand we replace the remaining elements of the system by a dispersion column which creates a degree of dispersion equivalent to the one caused by the real system.

We adopted for the dispersion column a one-parameter dispersion model defined by the following equation [26]:

$$\frac{\partial C_i}{\partial \omega} + \frac{\partial C_i}{\partial y} = \frac{1}{\mathrm{Pe}_{\mathrm{d}}} \cdot \frac{\partial^2 C_i}{\partial y^2} \quad (5)$$

In this equation, the Peclet number is defined by:

$$\mathrm{Pe}_{\mathrm{d}} = \frac{u_{\mathrm{d}} L_{\mathrm{d}}}{D_{\mathrm{d}}} \quad (6)$$

where u_{d}, L_{d} and D_{d} are the superficial velocity, the

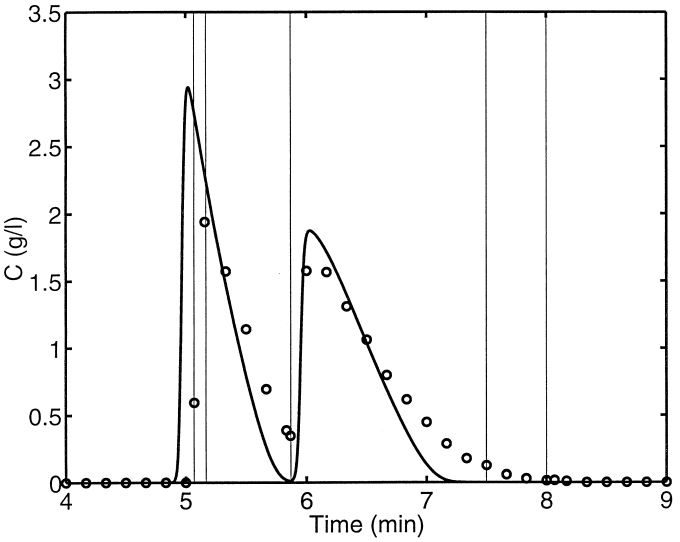

Fig. 7. Experimental (circles) and calculated (solid line) band profile for the initial pass of the racemate in the recycling setup. No extra-column dispersion included in the model. Mobile phase is ACN. $T=22$°C, flow-rate is 21.8 ml min^{-1}, injected volume is 5 ml with a concentration of 10 g l^{-1}, UV detection at 235 nm.

length and the axial dispersion coefficient in the dispersion column, respectively.

In Eq. (5), y is the dimensionless position variable defined as $y = l/L_d$, where l defines the axial position taken in the direction of the flow. The dimensionless time variable ω is defined as $\omega = u_d t/L_d$.

The initial condition employed in all the calculations was the one corresponding to a dispersion column containing no solute. The boundary condition at the inlet of the dispersion column is defined by the profile leaving the chromatographic column and the changes that it undergoes as a result of the

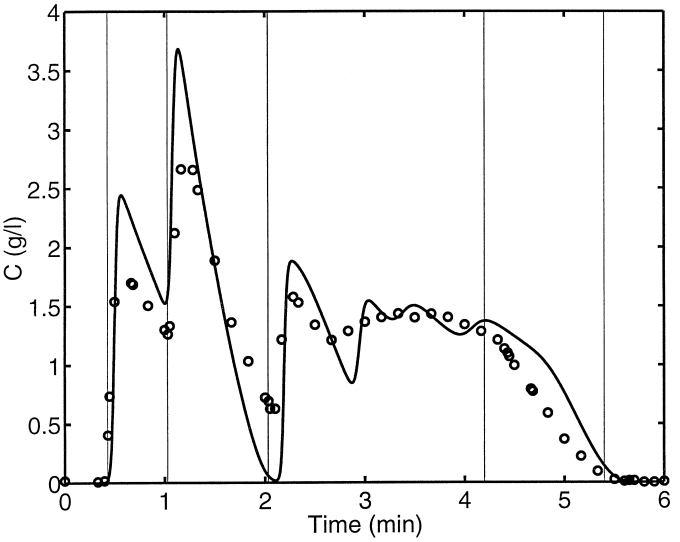

Fig. 8. Identical conditions as in Fig. 7 but results provided for Cycle 5.

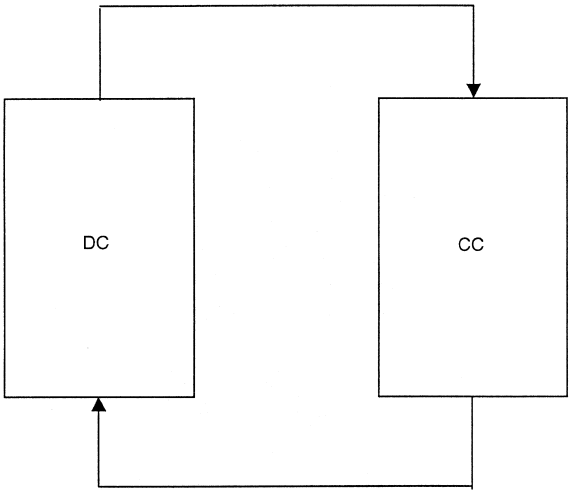

Fig. 9. Schematic diagram of the recycling setup within the context of the model including the chromatographic column (CC) and the dispersion column (DC).

fraction collection operations and of the injection of fresh sample. During the operation of the SSR process, the recycled part of the profile leaving the chromatographic column in the previous cycle and the fresh sample injected make up the boundary condition at the inlet of the chromatographic column for the calculation of the next cycle. The recycled part of the profile coming from the chromatographic column at the end of the previous cycle is split in two parts. The first part (first cut) goes to the top of the chromatographic column bypassing the loop (see Fig. 6). The second part (second cut) goes to the top of the chromatographic column through the loop in order to push the fresh sample contained there. So the first cut, the fresh sample and the second cut follow different pathways in the instrument. Accordingly, different parameters of the dispersion column should be selected for each of these three parts of the reinjected profile since they are affected by different delay times and degrees of dispersion. The results of the experiments (symbols) and the calculations (lines) for the initial pass and at the end of the 1st–10th cycles are presented in Figs. 10–20. The particular values of the parameters associated with the dispersion column are indicated in Fig. 10.

Eq. (5) was solved using a reported numerical scheme of integration based on finite differences [22]. The discretization leads to a system of linear equations which was solved using the routine F04FAF from the NAG library [27]. The stability

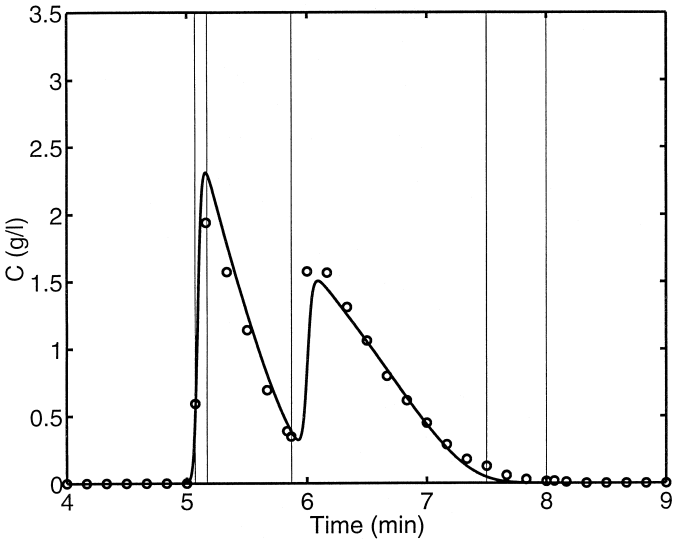

Fig. 10. Experimental (circles) and calculated (solid line) band profile for the initial pass of the racemate in the recycling setup. Extra-column dispersion included in the model. Mobile phase is ACN. $T=22°C$, flow-rate is 21.8 ml min^{-1}, injected volume is 5 ml with a concentration of 10 g l^{-1}, UV detection at 235 nm. The parameters of the dispersion column are: $L=19.5$ cm and $Pe=50$ for the first cut, $L=25.0$ cm and $Pe=50$ for the fresh sample, and $L=26.0$ cm and $Pe=50$ for the second cut. The diameter of the dispersion column is 1 cm in all cases.

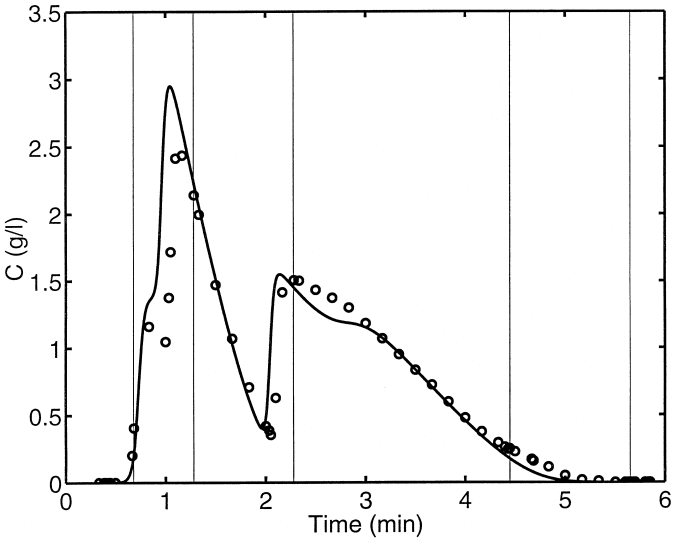

Fig. 11. Identical conditions as in Fig. 10 but results provided for Cycle 1.

conditions proposed by Rhee et al. [22] were also used.

4. Results and discussion

4.1. Adsorption equilibrium

The retention factors presented in Table 1 for the analytical and preparative columns are not significantly different. This is a reasonable result since both columns were packed with the same batch of packing material. Thus, the adsorption isotherm data determined with the analytical column should be useful for the prediction of overloaded band profiles in the preparative column.

When different adsorption capacities are assumed for the two enantiomers, the values of the two sets of

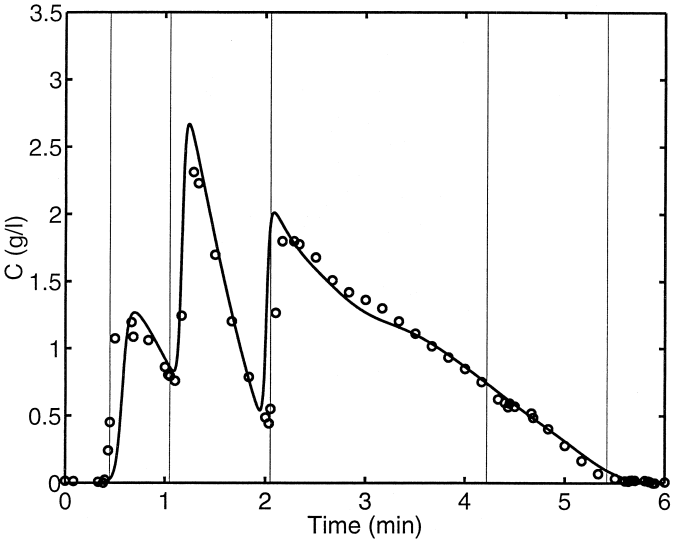

Fig. 12. Identical conditions as in Fig. 10 but results provided for Cycle 2.

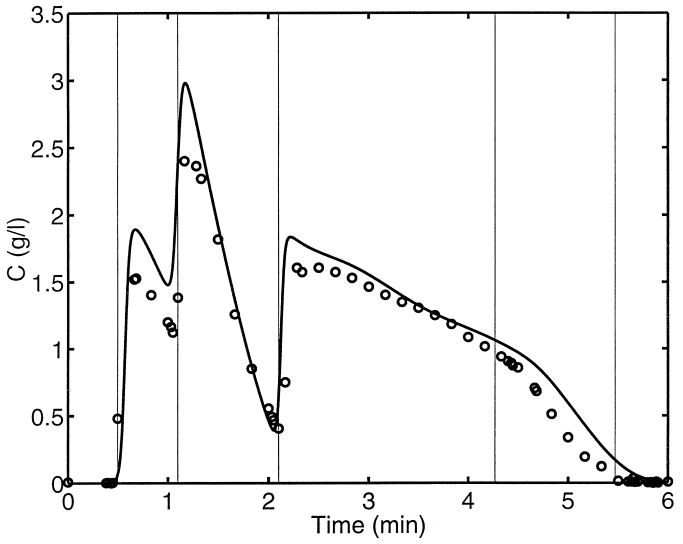

Fig. 13. Identical conditions as in Fig. 10 but results provided for Cycle 3.

parameters (n_2^{∞}, K_2^{L}) derived from the experimental data are very close for the second enantiomer (see Table 2). Note in Fig. 2(b) that the correlation of the single solute data of E2 (top curve) provided by the two sets of parameters is practically the same. On the other hand, the two sets of parameters differ somewhat for the first enantiomer (n_1^{∞}, K_1^{L}). The situation is clearly illustrated in Fig. 2(a), where the correlation of the single solute data given by the parameters obtained from the whole set of adsorption data deviates slightly at higher values of the concentration (top curve).

The adsorbed amounts corresponding to the competitive data of the second enantiomer calculated on the basis of the single solute parameters are also slightly underpredicted, as shown in Fig. 2(b) (bottom three curves, solid line). Note in Table 2 that the value of the residual sum of squares (RSS) between

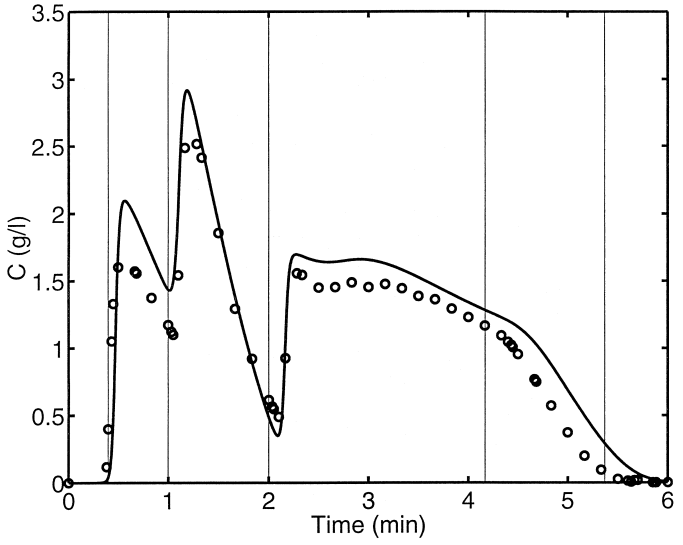

Fig. 14. Identical conditions as in Fig. 10 but results provided for Cycle 4.

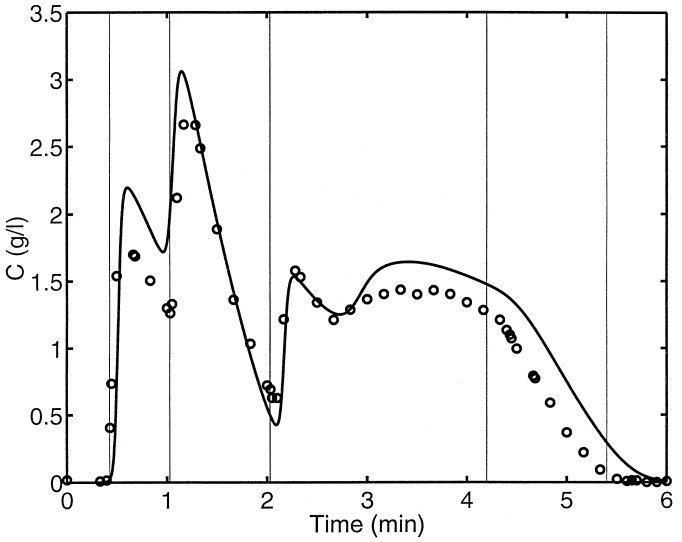

Fig. 15. Identical conditions as in Fig. 10 but results provided for Cycle 5.

the model estimates and the experimental data is higher when the model uses the single solute parameters. However, despite the slight deviations observed, both sets of parameters provide an adequate description of the adsorption data, as seen in Fig. 2.

When it is assumed that the two enantiomers have the same saturation capacity, the values of each parameter are similar among the three sets (see Table 3). Also, the prediction of the data corresponding to the second enantiomer [see Fig. 3(b)] is excellent and basically independent of the particular set of parameters employed. By contrast, the deviations between the model predictions and the experimental data are greater in the case of the first enantiomer, as shown in Fig. 3(a). The smallest deviations are, of course, produced by the parameters obtained from

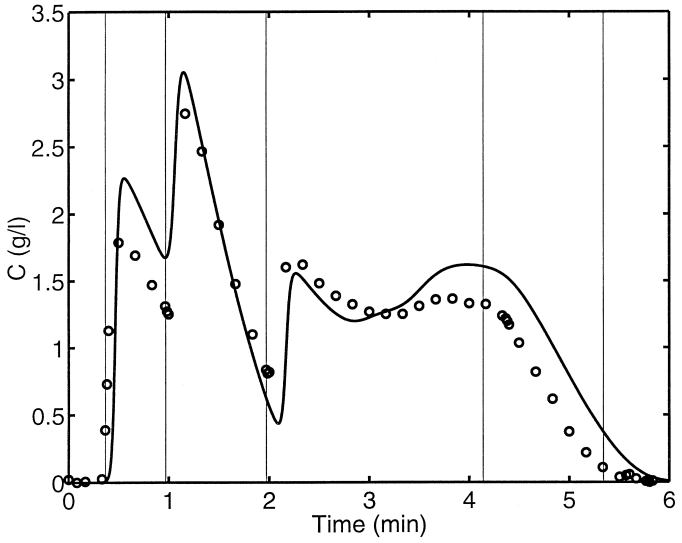

Fig. 16. Identical conditions as in Fig. 10 but results provided for Cycle 6.

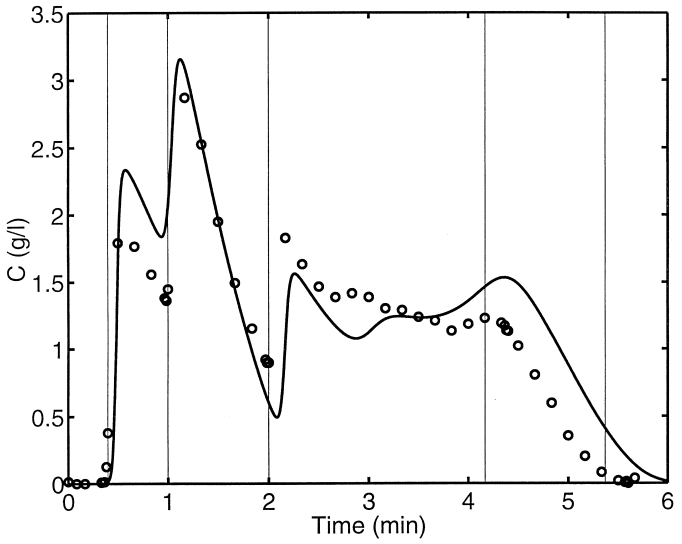

Fig. 17. Identical conditions as in Fig. 10 but results provided for Cycle 7.

the correlation of the whole set of adsorption data. The parameters obtained from the fit of the single solute data slightly underpredict the experimental adsorbed amounts for the binary mixtures. On the other hand the parameters obtained from the fit of the racemate data slightly overpredict them, specially the single solute data at higher concentrations.

It is understandable that the parameters obtained from the fit of the racemate data should deviate at higher concentrations. Recall that these correlations are basically interpolations valid within the range of concentrations studied. In the case of the racemate, the maximum experimental concentration employed for each enantiomer was 5 g l^{-1}. Thus, predictions of data beyond this value are likely to deviate. However, the fact that, in agreement with similar, earlier

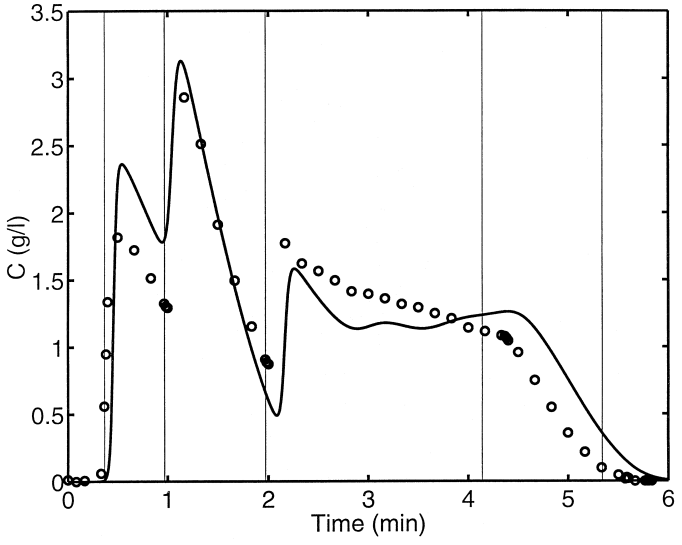

Fig. 18. Identical conditions as in Fig. 10 but results provided for Cycle 8.

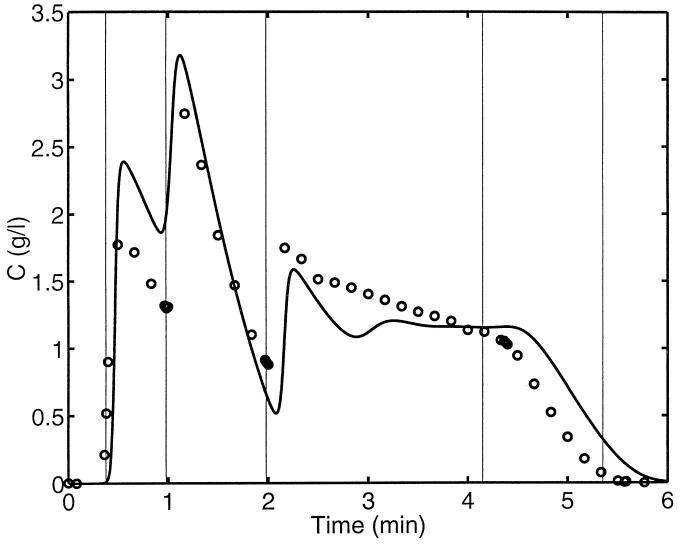

Fig. 19. Identical conditions as in Fig. 10 but results provided for Cycle 9.

findings [28–30], a reasonably good prediction of the adsorption surface can be obtained from the fit of the sole racemate data is extremely important from a practical point of view. In practice, pure enantiomers are often not available at the initial stages of the development of a particular separation. Accordingly, if the adsorption equilibria can be reasonably well approximated on the sole basis of the racemate adsorption data, the simulation of the separation can be performed in a straightforward fashion. The

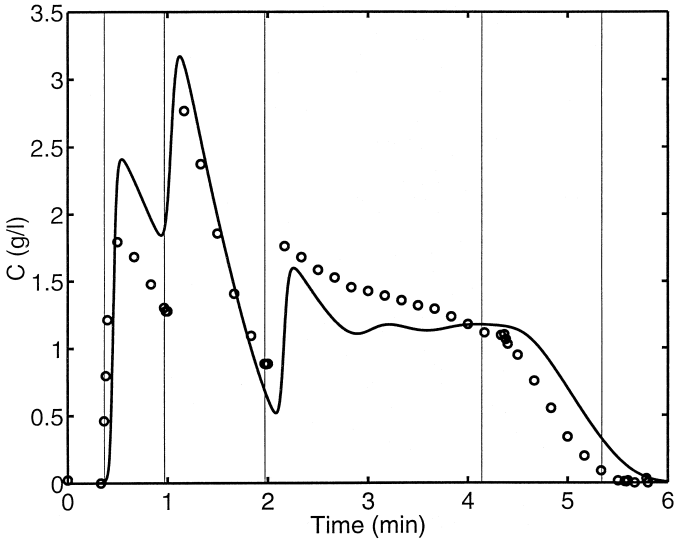

Fig. 20. Identical conditions as in Fig. 10 but results provided for Cycle 10.

model can then be used in the scale-up or optimization procedures. As a result, the time devoted to method development can be significantly reduced.

4.2. Band profiles

4.2.1. Analytical scale

Initially, we decided to calculate overloaded band profiles measured with the analytical column. We employed the equilibrium–dispersive model using the experimental injection profile as the boundary condition [31] and the competitive Langmuir isotherm, Eq. (1), with the parameters presented in Tables 1 and 2. Since we measured the total absorption signal rather than the individual band profiles, we converted the calculated total concentration of the concentration profiles into UV absorbance using a correlation polynomial. This second-order polynomial was derived from the correlation of the absorption signal associated with the FA plateaus and the corresponding total feed solute concentrations. Recall that the UV absorbance is the same for both enantiomers. The calculated profiles are presented in Figs. 4 and 5 (solid lines). Note the good description of the experimental data achieved by the model.

4.2.2. SSR cycles

The results obtained with the simpler model, which does not include any extra-column dispersion, are presented for the initial pass and for Cycle 5 in Figs. 7 and 8, respectively. Although the position of the shocks or band fronts on the time axis are properly predicted, the experimental band profiles show more dispersion, as expected.

Accordingly, the extra-column dispersion was included in the model, as illustrated in Fig. 9, in order to improve the prediction of the experimental results. The results of these calculations are presented in Figs. 10–20. Note the significant improvement achieved. In Fig. 21, we compare calculated and experimental profiles for the 20th cycle. Note that there remain a few features of the individual profiles that are not properly accounted for by the model. For example, the ‘‘tag-along ledge’’ [5] of the second enantiomer, which protrudes into the region of the first enantiomer, is not predicted by the model.

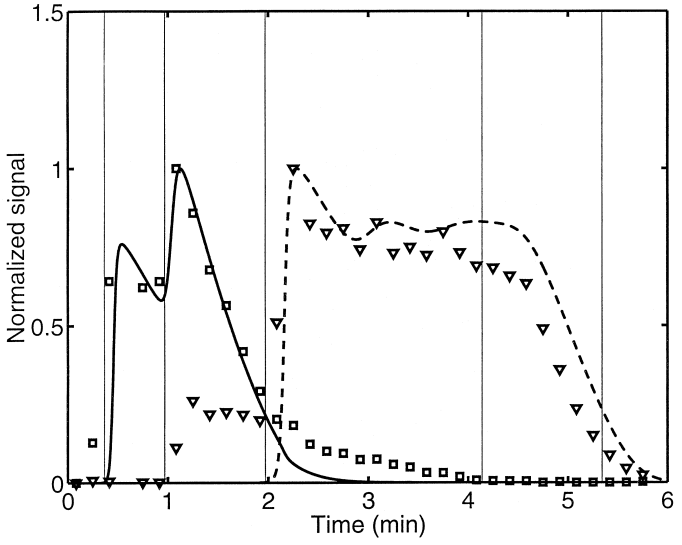

Fig. 21. Experimental (symbols) and calculated (lines) band profiles of E1 (squares and solid line) and E2 (triangles and dashed line) as obtained at the end of Cycle 20. Identical conditions as in Fig. 10. The ordinate was normalized for each enantiomer with respect to the maximum value of the integral among all the analyzed fractions (experimental) or with respect to the maximum value of the calculated concentration (theoretical).

As a result, the calculated individual profile of the second enantiomer overpredicts the experimental observations since an amount of the second enantiomer was not diverted to the region of the ''tag-along ledge''. The model basically predicts 100% purity of each enantiomer in the collected fractions (see Fig. 21). However, Table 4 shows that the purity of the collected fractions is less than 100%.

The intrusion of the first enantiomer into the band of the second enantiomer, although predicted by the model, is less pronounced than the one observed in practice. There is more dispersion in the central region of the profile than is predicted by the model.

There are several possible sources of additional dispersion which were not included in the model. First, dispersion and flow fluctuations, including flow pulsations, take place inside the column when the pump has to be stopped for some time and restarted at the end of each cycle [4,5]. Note that when the pump is stopped, the major part of the mixed region of the profile is located inside the chromatographic column. Second, mixing is possible in the ''T'' section joining the tubings coming from the MPR and the RV (see Fig. 6). Recall also that Fig. 6 shows only simplified schematics. In the actual setup, there are more valves and tubings that contribute to increase further the extra-column effects.

The exact reasons for which the agreement between calculated and experimental profiles in closed-loop SSR is only fair are important to find out, however. An exact knowledge of the profiles of the leading edge of the individual profile of E2 and the rear edge of the individual profile of E1 is critical to determine the windows for the collection of fractions. Still, the model as it is gives considerable insight into the matter. Additional safety factors can be assumed in order to recover fractions which are sufficiently enriched in E1 and E2. Minor adjustments turned out to be sufficient. Note that the prediction of the position of the shocks is excellent. The rear parts of the profiles are also reasonably well predicted.

Table 4
Analysis of fractions collected during the SSR run

Fraction	Cycles	% e.e.	
		E1	E2
1	0–6	99.5	0.0
1	7–11	99.3	0.0
1	11–15	99.1	0.0
1	16–20	99.4	0.0
2	0–5	–	98.9
2	6–10	–	99.3
2	11–15	–	99.0
2	16–20	–	99.0

4.3. Evolution to cyclic steady-state

As stated earlier, closed-loop SSR is a cyclic, one-column process similar to SMB chromatography. SMB reaches what is described as a periodic steady-state [15] or cyclic steady-state [16]. Although the SMB process is continuous, the injection and collection events do not occur at single points on the profile. Rather, in SMB, these events occur during a time window equal to the column switching time. During this time the profiles migrate by one column length. Thus the concentrations of the components in the two product streams oscillate in a saw-tooth pattern with a period equal to the column switching time [32]. The relative position of the injection point and the concentration profiles oscillates over a distance equal to one column length, again with a period equal to the column switching time. Thus the size, shape and composition of the SMB profile oscillates with a period equal to the column switching time. The ''amplitude'' of this oscillation decreases with increasing column number, and the SMB process approaches a true steady-state as the column number becomes large [15].

Likewise, closed-loop SSR reaches a periodic or cyclic steady-state. The profile size and shape of the bands of the two components change progressively, becoming smaller and losing mass during fraction collection, becoming broader due to the chromatographic separation process during the migration along the column, when fractions are not collected, and receiving new mass during injection. However, if one could observe the entire profile at a given time past the beginning of each period, one would observe that the profiles would become identical from cycle to cycle once steady-state is reached. Unfortunately, it is not possible to observe the concentration profiles at a given time. It is only possible to record their

passage at a given location. If one records the chromatogram with a detector during each cycle, one finds that the chromatogram evolves from cycle to cycle and tends toward a profile of constant size and shape. In other words, if one superimposes the chromatograms recorded during each cycle, one observes that, after a sufficient number of cycles, these chromatograms become virtually identical [4,5]. In Fig. 22 we present several experimental profiles while in Fig. 23 the same representation is given for the corresponding calculated profiles. Note that in both cases the system evolves toward the cyclic steady-state. Also, when this state is reached it is found that the amount of each component collected in the two fractions is equal to the amount injected during each cycle; that is, an overall cyclic mass balance develops.

5. Conclusion

The phase equilibria of the binary solute system studied here can be well represented by the competitive Langmuir model. The numerical values of the parameters of this model, derived either from the single solute, the multisolute, or the racemate adsorption data are reasonably close. This fact is extremely important from the practical point of view.

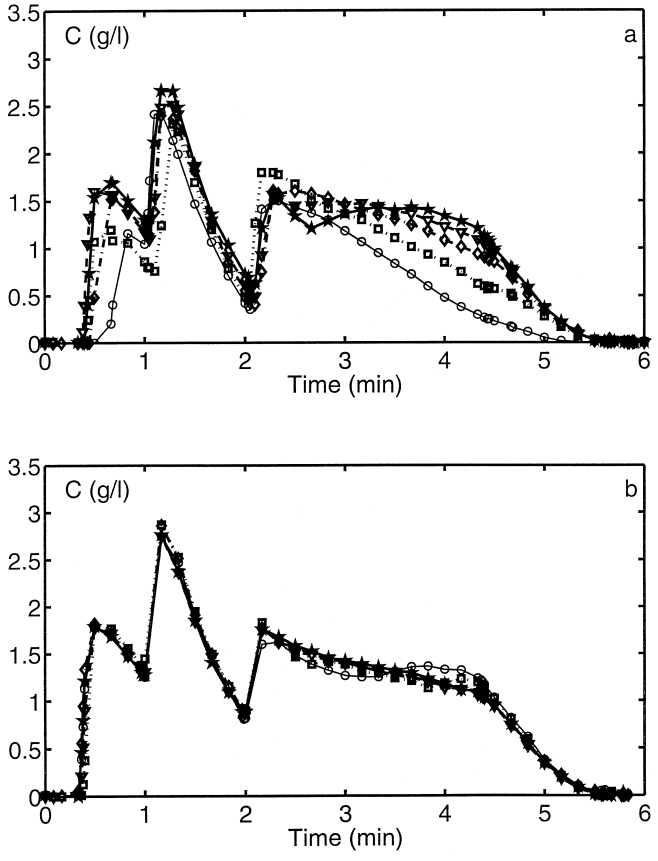

Fig. 22. (a) Experimental profiles for Cycles 1–5. Cycle 1, circles and thin solid line; Cycle 2, squares and dotted line; Cycle 3, diamonds and dash–dotted line; Cycle 4, triangles and dashed line; Cycle 5, stars and thick solid line. (b) Experimental profiles for Cycles 6–10. Cycle 6, circles and thin solid line; Cycle 7, squares and dotted line; Cycle 8, diamonds and dash–dotted line; Cycle 9, triangles and dashed line; Cycle 10, stars and thick solid line.

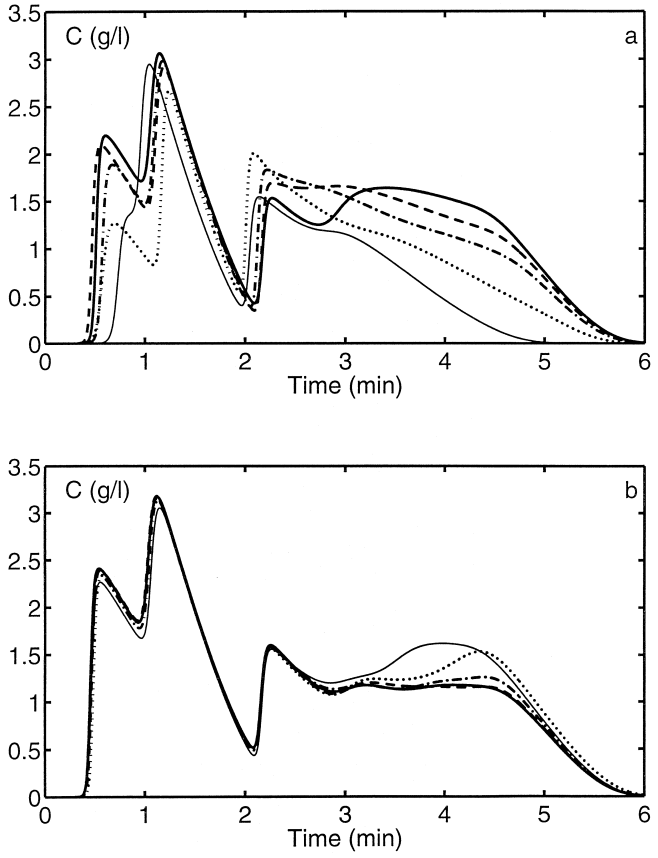

Fig. 23. (a) Theoretical profiles for Cycles 1–5. Cycle 1, thin solid line; Cycle 2, dotted line; Cycle 3, dash–dotted line; Cycle 4, dashed line; Cycle 5, thick solid line. (b) Theoretical profiles for Cycles 6–10. Cycle 6, thin solid line; Cycle 7, dotted line; Cycle 8, dash–dotted line; Cycle 9, dashed line; Cycle 10, thick solid line.

It means that a reasonable approximation of the two phase equilibria can be obtained from racemate adsorption data alone. For any enantiomeric system possessing this property, the process of method development, scale-up, and optimization can be carried out even before pure enantiomers become available.

The competitive Langmuir model and the equilibrium–dispersive model provide an accurate representation of the experimental, overloaded band profiles obtained at the analytical scale. At the preparative scale, our results demonstrate that a cyclic steady-state develops after several cycles. Then, the chromatograms remain virtually unchanged as long as the closed-loop SSR operation proceeds. Our model predicts the concentration histories at the detector and the composition of the fractions collected provided that extra-column dispersion is properly accounted for. This last condition is very important because extra-column contributions to band broadening are significant in this process. Using the model now validated, it is possible to develop an integrated framework for method development, scale-up, and optimization of SSR separations which is both theoretically sound and easy to implement experimentally.

Acknowledgments

The SSR processes are covered by patents and patent applications owned by NovaSep (France) and

licensed to CYBA Technologies, LLD (E. Greenwich, RI, USA). This work was supported in part by Grant CHE-97-01680 of the National Science Foundation and by the cooperative agreement between the University of Tennessee and the Oak Ridge National Laboratory. We acknowledge the support of Maureen S. Smith in solving our computational problems and fruitful discussions of this work MS with Marianna Kele.

References

[1] S.C. Stinson, Chem. Eng. News 73 (1995) 44.
[2] F. Charton, S.C. Jacobson, G. Guiochon, J. Chromatogr. 630 (1993) 21.
[3] F. Charton, M. Bailly, G. Guiochon, J. Chromatogr. A 687 (1994) 13.
[4] C.M. Grill, J. Chromatogr. A 796 (1998) 101.
[5] C.M. Grill, L. Miller, J. Chromatogr. A 827 (1998) 359.
[6] S. Jacobson, S.G. Shirazi, G. Guiochon, J. Am. Chem. Soc. 112 (1990) 6492.
[7] R.M. Nicoud, G. Fuchs, P. Adam, B.M. Bailly, E. Kusters, F.D. Antia, R. Reuille, E. Schmid, Chirality 5 (1993) 267.
[8] L.S. Pais, J.M. Loureiro, A.E. Rodrigues, J. Chromatogr. A 827 (1998) 215.
[9] A. Seidel-Morgenstern, G. Guiochon, Chem. Eng. Sci. 48 (1993) 2787.
[10] A. Seidel-Morgenstern, G. Guiochon, J. Chromatogr. 631 (1993) 37.
[11] A. Seidel-Morgenstern, G. Guiochon, AIChE J. 39 (1993) 809.
[12] B.E. Bidlingmeyer (Ed.), Preparative Liquid Chromatography, Journal of Chromatography Library, Vol. 38, Elsevier, Amsterdam, 1987.
[13] G. Guiochon, S.G. Shirazi, A.M. Katti, Fundamentals of Preparative and Nonlinear Chromatography, Academic Press, Boston, MA, 1994.
[14] M. Martin, F. Verillon, C. Eon, G. Guiochon, J. Chromatogr. 125 (1976) 17.
[15] F. Charton, R.M. Nicoud, J. Chromatogr. A 702 (1995) 97.
[16] M. Mazzotti, G. Storti, M. Morbidelli, J. Chromatogr. A 769 (1997) 3.
[17] E. Francotte, P. Richert, M. Mazzotti, M. Morbidelli, J. Chromatogr. A 796 (1998) 239.
[18] J.J. Jacobson, J. Frenz, Cs. Horvath, J. Chromatogr. 316 (1984) 53.
[19] J.J. Jacobson, J. Frenz, Cs. Horvath, Ind. Eng. Chem. (Res.) 26 (1987) 43.
[20] I. Langmuir, J. Am. Chem. Soc. 38 (1916) 2221.
[21] M.D. LeVan, T. Vermeulen, J. Phys. Chem. 85 (1981) 3247.
[22] H. Rhee, B.F. Bodin, N.R. Amundson, Chem. Eng. Sci. 26 (1971) 1571.
[23] P. Rouchon, P. Valentin, M. Schonauer, G. Guiochon, Sep. Sci. Technol. 22 (1987) 1793.
[24] F. James, M. Sepulveda, F. Charton, I. Quiñones, G. Guiochon, Chem. Eng. Sci. 54 (1999) 1677.
[25] A. Katti, Z. Ma, G. Guiochon, AIChE J. 36 (1990) 1722.
[26] H.S. Fogler, Elements of Chemical Reaction Engineering, Prentice Hall, Englewood Cliffs, NJ, 1992.
[27] NAG, The Numerical Algorithms Group, The NAG Fortran Library Manual, Mark 16, Downers Grove, 1993.
[28] S. Khattabi, D.E. Cherrak, J. Fischer, G. Guiochon, J. Chromatogr. A. submitted for publication.
[29] D.E. Cherrak, S. Khattabi, G. Guiochon, J. Chromatogr. A. submitted for publication.
[30] D. Burger, R. Neumüller, G. Yang, H. Engelhardt, I. Quiñones, G. Guiochon, Chromatographia, in press.
[31] I. Quiñones, J.C. Ford, G. Guiochon, Chem. Eng. Sci. 55 (2000) 909.
[32] T. Yun, G. Zhong, G. Guiochon, AIChE J. 43 (1997) 935.